RSC Advances

This is an *Accepted Manuscript*, which has been through the Royal Society of Chemistry peer review process and has been accepted for publication.
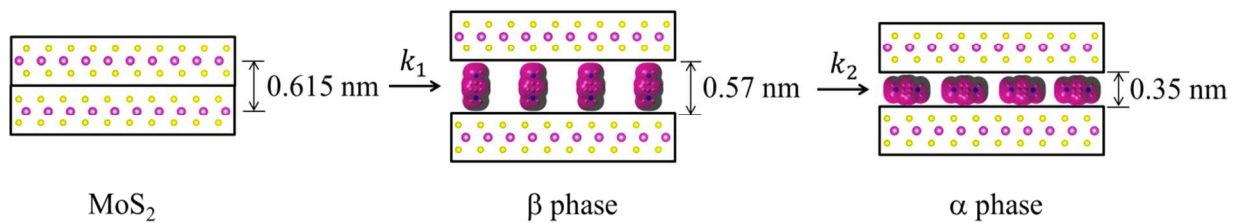
Accepted Manuscripts are published online shortly after acceptance, before technical editing, formatting and proof reading. Using this free service, authors can make their results available to the community, in citable form, before we publish the edited article. This *Accepted Manuscript* will be replaced by the edited, formatted and paginated article as soon as this is available.

You can find more information about *Accepted Manuscripts* in the **Information for Authors**.

Please note that technical editing may introduce minor changes to the text and/or graphics, which may alter content. The journal's standard **Terms & Conditions** and the **Ethical guidelines** still apply. In no event shall the Royal Society of Chemistry be held responsible for any errors or omissions in this *Accepted Manuscript* or any consequences arising from the use of any information it contains.

Table of contents entry

Color Graphic

$$MoS_2 \xrightarrow{k_1} \beta \text{ phase} \xrightarrow{k_2} \alpha \text{ phase}$$

MoS$_2$ ⟶ 0.615 nm k_1 0.57 nm β phase k_2 0.35 nm α phase

Text

A new intercalation mechanism is identified when electride solutions in ethylenediamine are used to generate MoS$_2$ intercalation compounds.

Use of amine electride chemistry to prepare molybdenum disulfide intercalation compounds

Amila Udayanga Liyanage, Michael M. Lerner*

Department of Chemistry, Oregon State University, Corvallis, OR 97331-4003, United States

Abstract

Electride solutions, formed by dissolution of Na(m) in ethylenediamine (en), are used to generate MoS_2 intercalation compounds. Two new intercalation compounds were obtained, labeled α and β phases, containing both Na and en as intercalate and cointercalate respectively. The intercalation reaction proceeds via formation of a kinetic product, the β phase, and subsequent generation of a stable thermodynamic product, the α phase. The β and α phases have interlayer distances, d_{IC}, of 1.19 and 0.97 nm, respectively, which are ascribed to a perpendicular or parallel orientations of en within the intercalate galleries. Product compositions, morphologies and spectrochemical features are obtained from thermogravimetry, SEM and Raman measurement. Electrochemical reduction of MoS_2 in an en-based electrolyte is investigated, but does not show the same intercalation reactions. The chemistry observed is compared with that previously reported for this and other MS_2 hosts, and with graphite intercalation.

Introduction

Many transition metal dichalcogenides (MX_2) are layered structures consisting of metal cations bound between hexagonal planes of chalcogenide anions.[1-3] The MX_2 layers can often be chemically[4-8] or electrochemically[9-11] reduced with concomitant intercalation of cationic guests, including the alkali metals,[4-6, 8] alkaline earths,[7] or other molecular or complex cations[1, 10]. The electrostatic attraction between the positive intercalates and the negative MX_2 layers stabilize these intercalation compounds.[1] In order to accommodate the cation guests, the MX_2 sheets separate, with the interlayer expansion, Δd, defined as:

$$\Delta d \ = \ d_{IC} \ - \ d_h \tag{1}$$

where d_{IC} and d_h are the interlayer repeat distances observed for the intercalation compound and the MX_2 host, respectively. (Fig.1) The many possible relative dispositions of chalcogenide planes leads to a rich variety of identified MX_2 structures and polytypes. The transition metal cations may have either trigonal prismatic or octahedral chalcogenide coordination. Some commonly observed arrangements are represented by 1T-TiS_2 with an $(AbC)_n$ stacking repeat, 2H-TaS_2 with an $(AbACbC)_n$ stacking repeat, and 2H-MoS_2 with an $(AbABcB)_n$ stacking repeat.

1T-TiS$_2$ has octahedral coordination, whereas 2H-TaS$_2$ and 2H-MoS$_2$ have trigonal prismatic coordination around transition metal cations.[1-3]
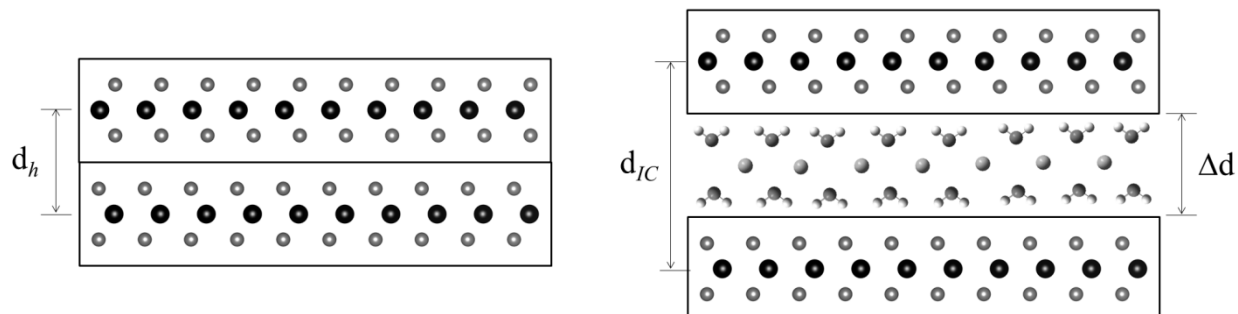

Figure 1: Schematic representations of MoS$_2$ and Na$_x$MoS$_2$·δH$_2$O, where H$_2$O is a cointercalate.

MoS$_2$ is a rather chemically inert semiconductor, and is highly anisotropic, with an electrical resistivity 1000x greater in the direction perpendicular to the sheets. Important applications include use as a solid lubricant in both terrestrial and space environments (where graphite shows poor performance), as a catalyst in hydrodesulfurization and hydrogen evolution reactions, and as a photochemical catalyst in the oxidation of organics. MoS$_2$ holds promise for more efficient solar cells due to its resistance to photodegradation in water and photochemical activity over a wide frequency range.[3]

Intercalation by alkali metal cations and co-intercalates can change MoS$_2$ from a semiconductor to a metal.[3] For example, the band gap decreases and the electrical conductivity increases by formation of Li$_{0.1}$MoS$_2$.δ(PEO)[12] and Li$_{0.1}$MoS$_2$·δdialkylamine[13], which both act as mixed electronic-ionic conductors. Intercalation chemistry may thereby enable tailored conductivities for specific materials applications. Some alkali metal or alkali earth metal intercalation compounds with MoS$_2$ are superconducting, with transition temperatures typically ~7°K.[7, 8]

Intercalation of promoter elements like Co or Ni has improved the catalytic activity of γ-Al$_2$O$_3$-supported MoS$_2$ in hydrodesulfurization.[3] Enhanced hydrogen evolution catalysis has been reported by use of metallic 1T-MoS$_2$ nanosheets obtained via chemical exfoliation of 2H-MoS$_2$ nanostructures grown directly on graphite.[14]

MoS$_2$ and its intercalation compounds may also be useful as electrodes in energy storage. Lemmon et al have reported improved Li cycling stability and a significant increase in reversible capacity for the PEO/MoS$_2$ and PEO/MoS$_2$/graphene composites.[15, 16] MoS$_2$, MoS$_2$/graphene composites and MoS$_2$ nanosheets have recently been explored for use in Na-ion batteries where cycling performance is highly correlated to the nanostructure.[17-19]

Several synthetic routes have been used to produce A_xMX_2 intercalation compounds where A is an alkali metal, including; (1) direct high temperature solid state synthesis by combining either the MX_2 host and an alkali metal or combining the A, M and X constituent elements[1, 2], (2) reaction of the MX_2 host with a reductant solution[4-7], or (3) electrochemical reduction of the MX_2 host in a suitable electrolyte[9, 11]. For some metal redox couples, such as Mo(IV)/Mo(III), the intercalation reaction requires powerful reductants such as an alkali metal dissolved in liquid ammonia.[4, 5, 8] This blue electride solution contains sodium ion complex cations and solvated electrons which are a powerful reductant[20]:

$$M(s) \quad \xrightarrow{NH_3} \quad [M(NH_3)_6]^+ (solv) \; + \; e^- (solv) \qquad\qquad (2)$$
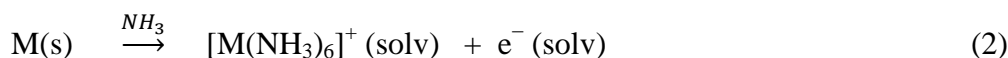
Other strong reductants that have been used to form A_xMX_2 include butyllithium or sodium naphthalide dissolved in suitable organic solvents.[1, 6] For MX_2 hosts with more easily reduced metal cations, intercalation can be accomplished using ammonia[2, 21, 22], amines[1, 2, 23-26] or aqueous solutions[27].

In some cases, solvent (Sol) cointercalation is observed (Fig. 1), to generate compounds represented as $A_xMX_2 \cdot \delta Sol$. The driving force for such cointercalation is the retention of some solvation of the alkali metal intercalate.

Alkali metal intercalation of MS_2 was first reported in 1959.[4] Rüdorff has reported a wide range of A_xMX_2 intercalation compounds with the hosts including MoS_2, $MoSe_2$, WS_2, WSe_2, ReS_2, TiS_2, and $TiSe_2$.[4, 5] Rouxel and coworkers have also extensively studied intercalation of the group 4 transition metal MX_2 compounds.[2] Whittingham et al studied the lithium intercalation of MX_2s[6] and Schöllhorn et al reported several different syntheses and exchange reactions for MX_2 intercalation compounds.[1, 28]

Rüdorff reported formation of $Li_{0.8}MoS_2 \cdot 0.8NH_3$, $Na_{0.6}MoS_2$, $K_{0.6}MoS_2$ and $Cs_{0.5}MoS_2$ compounds with interlayer expansions (Δd, eqn 1) of 0.335, 0.135, 0.195 and 0.274 nm, respectively.[5] Since the ionic radius of Li^+ is ≈ 0.076 nm[29], the much larger expansion of $Li_{0.8}MoS_2 \cdot 0.8NH_3$ indicates the presence of NH_3 cointercalate. Schöllhorn and Weiss reported that these intercalation compounds can also absorb water to form hydrated cation complexes with an increase in Δd to 0.29 – 0.70 nm, depending on the reaction conditions.[28]

A series of alkali metal and alkaline earth intercalation compounds of MoS_2 were synthesized in $NH_3(l)$, with the observed Δd values ranging from 0.14 to 0.37 nm.[7, 8] The same method was utilized to synthesize intercalation compounds for TaS_2, with the resulting products Na_xTaS_2 and K_xTaS_2 giving Δd of 0.11 and 0.21 nm, respectively.[30]

Li_xTiS_2, Li_xMoS_2, and Li_xTaS_2 were obtained by reaction of the hosts with butyllithium in hexane, with Δd from 0.025–0.05 nm.[6]

Some organic and inorganic Lewis bases react to form intercalation compounds with groups 4 and 5 MX_2 hosts with Δd ranging from 0.30 nm (for smaller molecules like NH_3) to 5.23 nm (for octadecylamine), with compositions reflecting the uptake of 0.1 to 1.0 guests per MX_2 unit.[2] This interaction between the host and guest has been ascribed either to charge transfer[1] or to a redox reaction where the host is reduced and the cationic form of base, solvated by the neutral base, intercalate (i.e. NH_4^+ and NH_3 respectively). Group 6 chalcogenides hosts do not react to form intercalation compounds with organic bases in this manner.[1,2]

Some MX_2 hosts react in strong aqueous base to intercalate hydrated alkali metal cations, e.g. $Na_{0.3}TaS_2 \cdot \delta H_2O$.[2,27] These complex intercalates undergo facile displacement by subsequent reaction with aqueous salt solutions.[28] Alternately, the water cointercalate can be displaced by reaction in polar inorganic or organic solvents.[28] The product compositions, including both the contents of intercalate cations and of cointercalates, depend on the degree of reduction, exposure to exchange solutions, and post-reaction processing.

Ethylenediamine (en) and trimethylenediamine (tn) react directly with TiS_2, NbS_2, and TaS_2 to form intercalation compounds with $\Delta d = 0.34$–0.41 nm. From the known intercalate dimensions, these gallery dimensions indicate that the amine intercalates must form monolayers with long molecular axes oriented parallel to the host layers.[24-26] These products show a range of compositions depending on the host and sample processing conditions, with intercalate to MX_2 ratios of 0.17–0.39 for en and 0.15–0.33 for tn. Secondary amines, such as diethylamine, dibutylamine, and dipentylamine react with exfoliated MoS_2, generating $Li_{0.1}MoS_2 \cdot \delta$ dialkylamine, where $\delta = 0.11$-0.42 and $\Delta d = 0.374$–0.445 nm, depending on the dialkylamine cointercalate.[13]

Our group has previously explored the use of electride solutions to prepare graphite intercalation compounds containing amines or diamine intercalates.[31-34] Stage 1 and 2 graphite intercalation compounds (GICs) were reported for syntheses using Li(m) or Na(m) dissolved in liquid en. When the intercalate is the $Li(en)^+$ complex, the intercalate guests show an orientation transition of perpendicular to parallel upon evacuation. With $Na(en)^+$, the complexes show only a parallel orientation.[33]

Since the reduction of graphite generally occurs at a lower potential than that for MoS_2, it is worthwhile to explore electride reactions for the intercalation of dichalcogenide hosts, especially since alkali metal-amine electride systems (other than with ammonia) have not previously been reported. In this work, we describe the first use of electride solutions to form MoS_2 intercalation compounds with amines, along with the product structures and compositions obtained. A novel intermediate phase is found, and we propose a mechanism for the reaction. The results obtained are also analyzed in light of recent reports on electrochemical reduction of MoS_2.

Experimental

Reagents

Sodium metal (3-12 mm pieces in oil, 99.95 %, Alfa Aeser), ethylenediamine (en) (99%, Alfa Aeser), molybdenum disulfide (MoS_2) (powder <2 micron, 99%, Aldrich), poly(ethylene-*co*-propylene-*co*-5-methylene-2-norbornene) (EPDM) (Aldrich), acetylene black (99.5+%, Alfa Aeser), cyclohexane (ACS grade, Alfa Aeser), sodium hexafluorophosphate ($NaPF_6$) (98%, Aldrich) and acetonitrile (HPLC grade, Fisher Scientific) were used as received.

Chemical Syntheses

Synthesis and handling of the air-sensitive reagents were performed under an inert atmosphere (N_2) using either a drybox or septum-syringe techniques. In a typical reaction, Na metal (50 mg) was stirred overnight in ethylenediamine (3.0 mL) at 60°C under an inert (N_2) atmosphere to form a blue-colored electride solution. MoS_2 (100 mg) was then added to the electride solution, and the reaction vigorously stirring at 60°C for 48 h. Samples were centrifuged for 10 min and the solution phase was extracted by syringe. The solid products were placed under vacuum for 12 h at 60°C.

As specified below, the above reaction conditions (time, temperature, reagent amounts and chemical addition sequence) were varied for some experiments. Products obtained are labeled with reaction temperature and time. For example, the sample obtained by reaction at 60°C for 24 h has been labeled "S-60C-24h".

Electrochemical syntheses

Galvanostatic reduction was performed in a 2-compartment cell with a fritted glass separator maintained under an inert (N_2) atmosphere at ambient temperature. Working electrodes were prepared by painting SS mesh (geometric area ~1 cm^2) with a cyclohexane slurry containing MoS_2 powder (80 mass pct.), acetylene black (15 mass pct.), and EPDM binder (5 mass pct.). The dried electrode mass was 18-20 mg. Counter and reference electrodes were SS mesh and SS wire. The electrolyte solution was 0.1 M $NaPF_6$ in ethylenediamine. Working electrodes were reduced at a constant current of 0.10 mA for 16–48 h, then immediately removed from the cell, rinsed briefly with 3–4 mL of acetonitrile, and dried overnight under vacuum at ambient temperature.

Analyses

Powder X-ray diffraction (XRD) data from 3–20°2θ were collected on a Rigaku MiniFlex II diffractometer, using Ni-filtered Cu K$_\alpha$ radiation, at a scan rate of 3°/min and step size of 0.02°. Diffraction peak areas were obtained using MDI JADE 9.0 XRD analysis software.

Thermogravimetric (TGA) analyses were performed using a Shimadzu TGA-50 analyzer under flowing Ar gas (20 mL/min) from ambient to 400°C at a heating rate of 10°C/min and under air from ambient to 900°C at a heating rate of 10°C/min. Scanning electron micrographs (SEM) were obtained using an FEI Quanta 600F scanning electron microscope equipped with a field emission gun and operated at 10 kV. Raman spectra were obtained from 60–4000 cm^{-1} using a Witec Alpha 300 confocal Raman microscope with 514 nm laser source.

The van der Waals volume of en, V_{en}=0.0651 nm^3 was calculated based on Bondi radii using a method termed "Atomic and Bond Contributions of van der Waals volume" (VABC).[35] Volume of Na$^+$, V_{Na}=0.00445 nm^3 was calculated using the ionic radius of Na$^+$ (0.102 nm).[29] Packing fractions for MoS$_2$ intercalation compounds were calculated[36, 37] as:

$$Packing\ fraction = 2\ (nV_{Na} + mV_{en})\ /\ \sqrt{3}a^2\Delta d \qquad (3)$$

where n and m are the molar ratios of Na:MoS$_2$ and en:MoS$_2$ respectively, and a=0.3160 nm[1, 2].

Energy optimization of the gas-phase en molecule was performed using the DFT B3LYP method with a 6-31G+(d,p) basis set and Gaussian 09W software.

Results and Discussion

The powder XRD patterns obtained from reactions of MoS_2 with a sodium electride solution (Figs. 2,3) shows host expansion to form new intercalation compounds. In Fig. 2 (S-60C-48h), a single new phase is evident with interlayer distance, d_{IC}=0.97 nm. The expansion relative to the host MoS_2 sheet thickness (d_{002}=0.615 nm)[3] is Δd=0.35 nm. Hereafter this new phase is labeled the α phase.
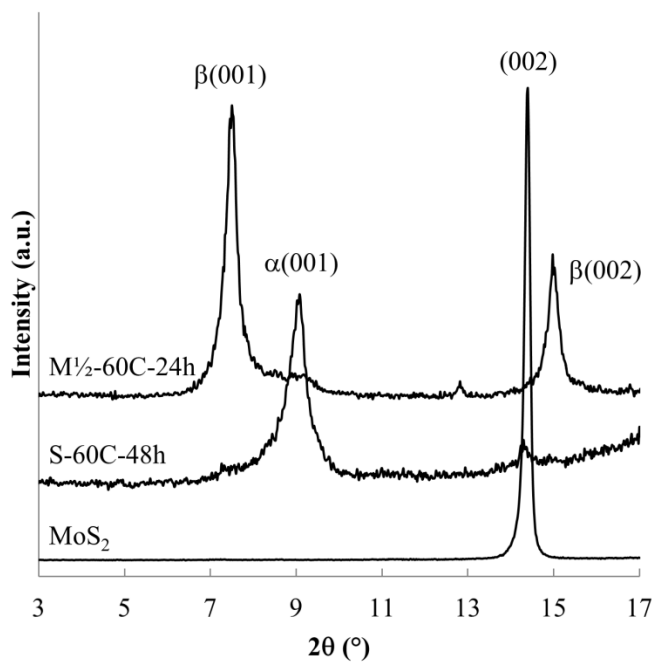

Figure 2. Powder XRD of MoS_2 and the intercalation compounds obtained after 48 h reaction at 60°C (S-60C-48h) and after 24 h reaction at 60°C using decreased Na mass (M½-60C-24h).
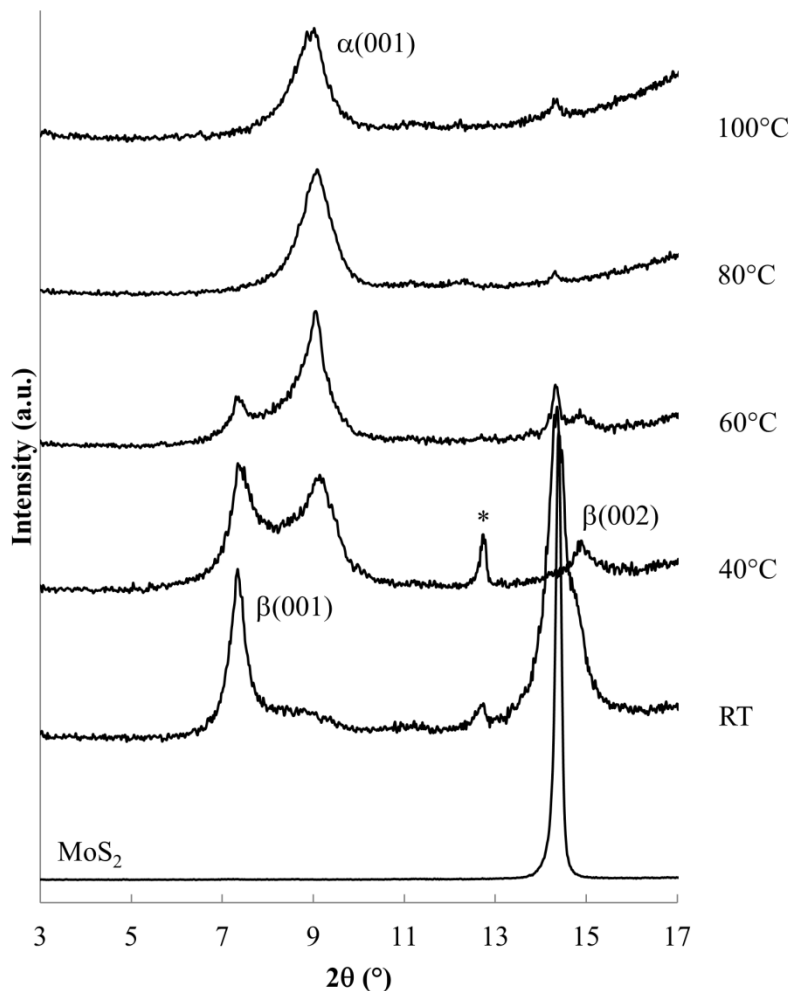
Figure 3. Powder XRD of MoS_2 and the intercalation compounds obtained after 24 h at reaction temperatures ambient to 100°C.

Fig. 3 shows XRD patterns obtained after 24 h reaction at ambient to 100°C. Ambient temperature reaction produces a different new phase (with d=1.19 nm, Δd=0.57 nm), labelled the β phase, along with the unreacted host. Reaction products at 40 and 60°C contain both the α and β phases along with unreacted MoS_2. Higher temperature reactions, at 80°C and 100°C, produce mainly the α phase, with a very small residual of unreacted MoS_2.

Lower temperature reactions show an additional diffraction peak (tagged with an *) near d=0.69 nm, attributed to Na_xMoS_2, i.e. the intercalation product without the en cointercalate. This phase has previously been reported, with d=0.75 nm[28] or d=0.71 nm[38]. The small interlayer expansion observed for this phase (Δd≈0.1 nm) eliminates the possibility of en contained in that product.

Summarizing the changes observed with varied reaction temperature, (i) lower temperature reactions result in a relatively large amount of unreacted host (an incomplete reaction), and are relatively rich in the β phase, and (ii) higher temperatures generate nearly complete reactions to form mainly the α phase.

The incomplete reactions observed at lower temperature could arise from the slow kinetics of amine electride (reactant) formation, resulting in a low reductant concentration, or alternately they may be related to a slower rate of diffusion of the $Na(en)_x^+$ complex intercalate into the intercalation compound galleries.

In other experiments aimed at decreasing the electride reactant concentration, reactions for 48 h reaction at 60°C were run using ½ the mass of Na or 5x the standard volume of en. Both changes results in products containing both the α and β phases and unreacted MoS_2. The association of β phase and incomplete reactions again provides some evidence that the β phase is a kinetic product. In one experiment using the decreased Na mass, the product obtained after 24 h reaction at 60°C contained only the β phase (Fig. 2. M½-60C-24h).

Products obtained at 60°C with varied reaction times are shown in Fig. 4. Shorter reaction times produce the β phase along with unreacted MoS_2; the α phase is first evident after reaction for 1 h. At longer reaction times, the β phase and MoS_2 are no longer observed. These data confirm that the β phase is formed more rapidly as a kinetic product, but ultimately disappears as the more stable α phase forms.
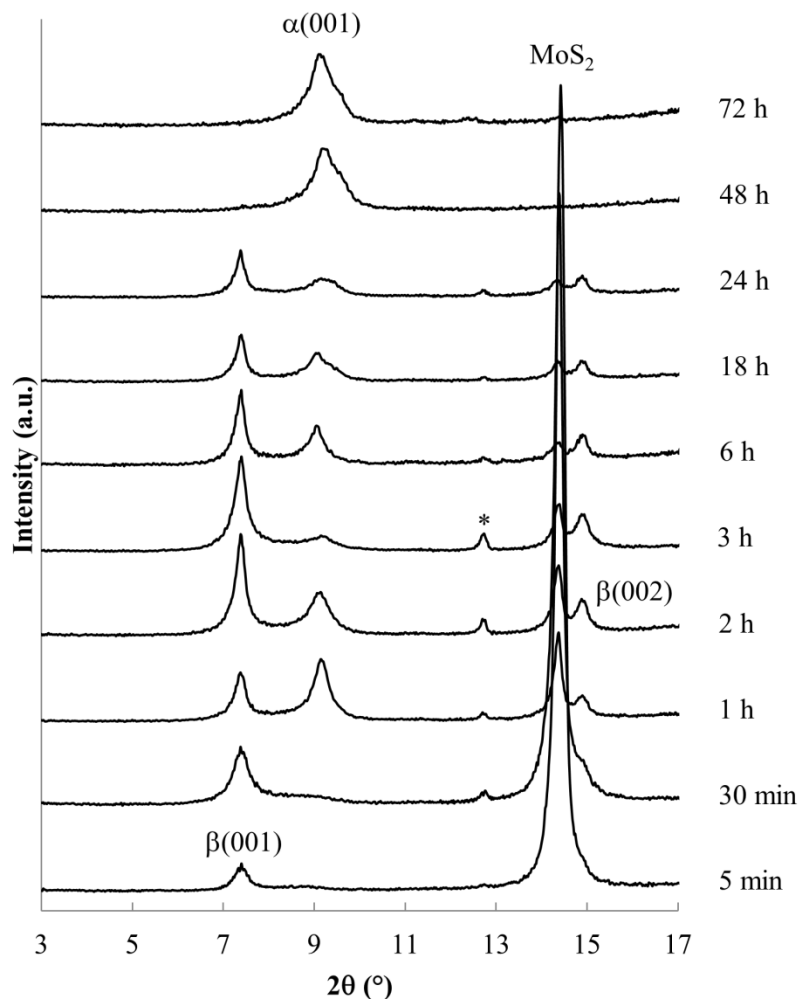
Figure 4. Powder XRD data obtained for reaction of MoS_2 with Na/en electride solution at 60°C. Reaction times are indicated at the right.

Relative PXRD peak areas (A/A_t) were obtained by dividing the raw area of individual peak (A) by the total area of all observed peaks ($A_t=\Sigma A$), to normalize relative peak areas and more closely represent the volume fraction of the associated phases. Analysis of relative PXRD peak areas (A/A_t), shown in Fig. 5, shows clearly the intermittent appearance of the β phase during the 60°C reaction.
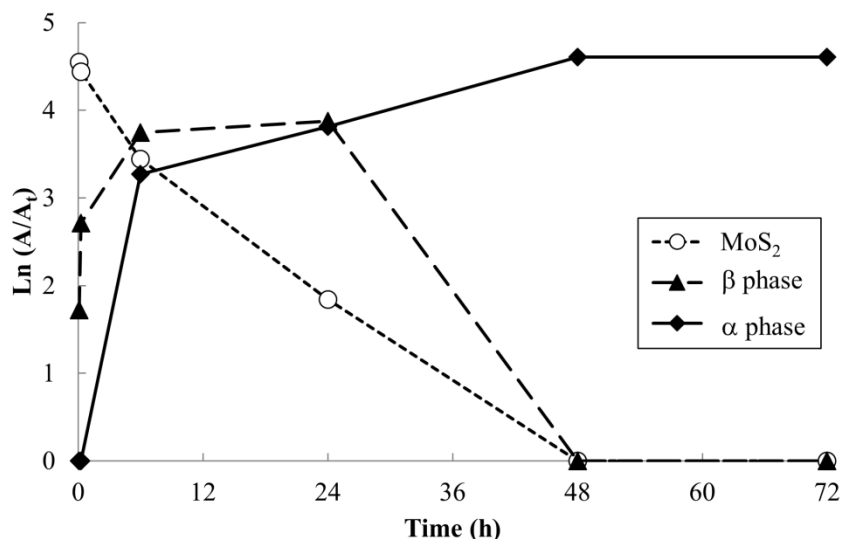
Figure 5. Ln(A/A$_t$) vs. reaction time at 60°C.

Although lower electride concentrations, lower reaction temperatures and shorter reaction times are seen to favor formation of the β phase, this phase was difficult to obtain as a single-phase product. This indicates that the rates of conversion of MoS$_2$ to β phase, and β to α phase, i.e. rates k_1 and k_2 in Fig. 6, were comparable under the range of reaction conditions studied.
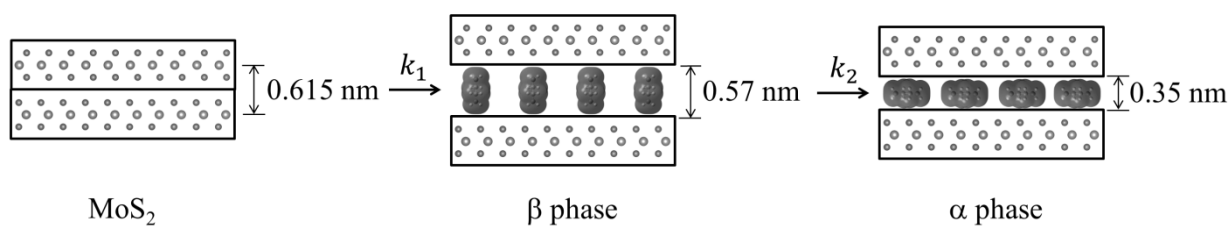

Figure 6. Proposed reaction mechanism; MoS$_2$ forms a metastable β phase, which converts to the more stable α phase.

We propose that the β phase appears due to the more rapid diffusion of the Na(en)$_x^+$ complex with a perpendicular orientation within intercalate galleries. Thermodynamic stabilities of these products depend on several factors, such as electrostatic and solvation enthalpies. Smaller galleries, as observed for the α phase, should generally have a more favorable lattice enthalpy, since E∝– 1/d.

The α and β phases obtained are both ascribed to the cointercalation of en with Na$^+$ to form an intercalate monolayer. The α phase expansion (Δd=0.35 nm) corresponds to an en orientation with long axis parallel to host sheets, and the β phase expansion (Δd=0.57 nm) to a perpendicular en orientation. Optimized molecular dimensions obtained by Gaussian (Fig. 7) correlate well with the observed gallery dimensions. Amine intercalates have been previously reported with Δd=0.37–0.40 nm for MS$_2$ hosts[13, 26], but we are not aware of any reports on the observed β phase for any MX$_2$ intercalation products. Graphite intercalation compounds (GICs) containing en show both types of expansion, with the perpendicular orientation of Δd=~0.5 nm for LiC$_x$·δen and a reported transition to parallel orientation observed upon evacuation of the product.[33] That work also reported the formation of a GIC with composition NaC$_{15}$·1.0en with Δd = 0.36 nm, indicating a parallel en orientation.[33]
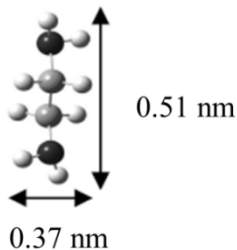

Figure 7. Gaussian-optimized molecular dimensions of ethylenediamine.

An alternate explanation for the appearance of α and β phases could be the formation of en monolayers and bilayers, respectively, as occurs in the hydration of A$_x$MS$_2$.[39] However, thermogravimetric data (*vide infra*) show that the obtained phases have similar en content, which does not support this model. Additionally, the observed d$_{IC}$ for the α phase is 1.19 nm, which is significantly less than the 1.32 nm calculated to accommodate two en layers.
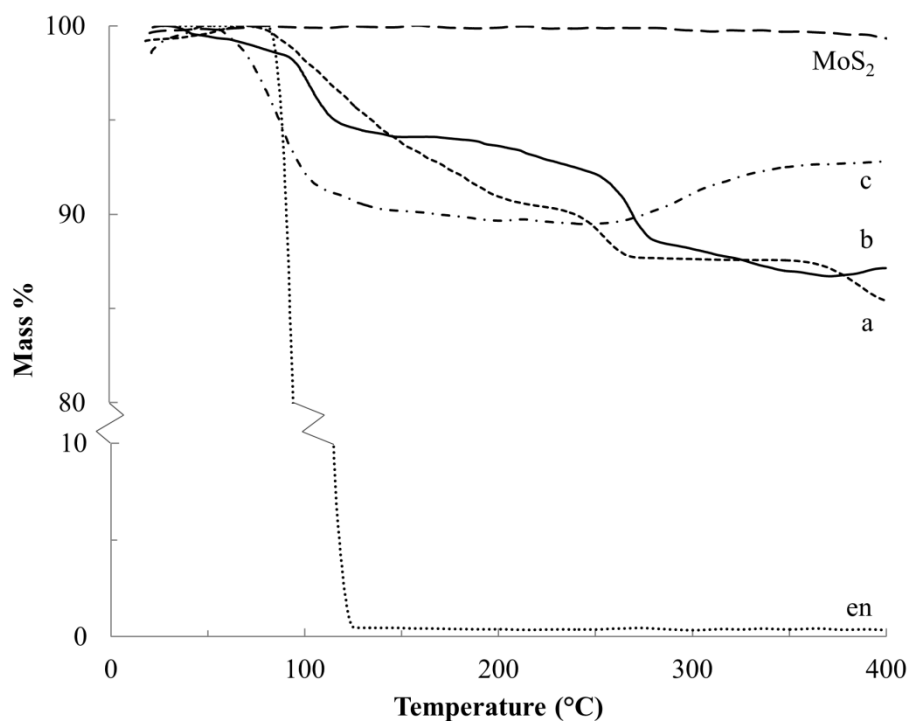
Figure 8. Thermograms of MoS_2, en, (a) the α phase Na-en-MoS_2 intercalation compound (S-60C-48h) and (b) a β phase predominant product (S-60C-3h) under Ar flow, and (c) β phase predominant product (S-60C-3h) analyzed under air flow.

Thermograms for the Na-en-MoS_2 intercalation compounds under Ar flow (Fig. 8a, b) show two mass loss events at 100–200°C and 225–275°C, which are attributed to volatilization (b.p. of en = 116°C) and decomposition of the en cointercalate. Under air flow, a mass increase above 275°C can be attributed to the formation of Na_2O (Fig. 8c). From the mass loss and uptake, the composition for S-60C-48h (α-phase) and S-60C-3h (β-phase predominant) are found to be $Na_{0.3}MoS_2 \cdot 0.4$en and $Na_{0.2}MoS_2 \cdot 0.3$en, respectively. Other studies of MS_2 (M=Ti, Ta and Nb) also give maximum en:MS_2 ratios in the 0.3-0.4 range.[24-26]

Where all graphene sheets are separated by intercalate galleries (i.e. in the stage 1 products), GIC have an en mass of 20–22%.[33] In comparison, the structurally-analogous MoS_2 intercalation compounds show en contents of ~12%. Calculated packing fractions (Table 1) correcting for the different host sheet surface areas and formula masses, indicate much denser intercalate packing for both α and β phases in MoS_2 than for the corresponding orientations in GICs. In part, this reflects a higher en:Na ratios in MoS_2 intercalation compounds (1.3-1.5 in MoS_2 compounds vs. 0.6-1.0 in stage 1 GICs[33]). Also, the packing fraction of β phases is lower due to the greater gallery expansion.

Table 1. Compositional data for en containing intercalation compounds

Composition	Stage	Phase	Packing fraction	Reference
$LiC_{15} \cdot 0.8en$	1	α	0.40	33
$LiC_{26} \cdot 0.7en$	2	β	0.28	
$NaC_{15} \cdot 1.0en$	1	α	0.51	
$NaC_{25} \cdot 0.6en$	2	α	0.40	
$Na_{0.3}MoS_2 \cdot 0.4en$	1	α	0.88	This work
$Na_{0.2}MoS_2 \cdot 0.3en$	1	β	0.43	

Less dense packing in the β-phase may facilitate $Na(en)_x^+$ complex diffusion, allowing more rapid formation of this phase. It may also be that the very high packing density in the α-phase MoS_2 compound prohibits reduction to the extent observed where no en cointercalate is present (such as in $Na_{0.6}MoS_2$)[4, 5].

The calculated sheet charge densities for $NaC_{15} \cdot 1.0en$, $Na_{0.3}MoS_2 \cdot 0.4en$ and $Na_{0.2}MoS_2 \cdot 0.3en$ are 2.5, 3.5, and 2.3 e^-/nm^2, respectively. Again, we can propose that lower charge densities may allow for more rapid diffusion, but result in a less thermodynamically stable product.

SEM images (Fig. 9) show that a layered microstructure is retained in all samples, with the reaction products displaying a somewhat delaminated appearance as compared to the starting MoS_2.
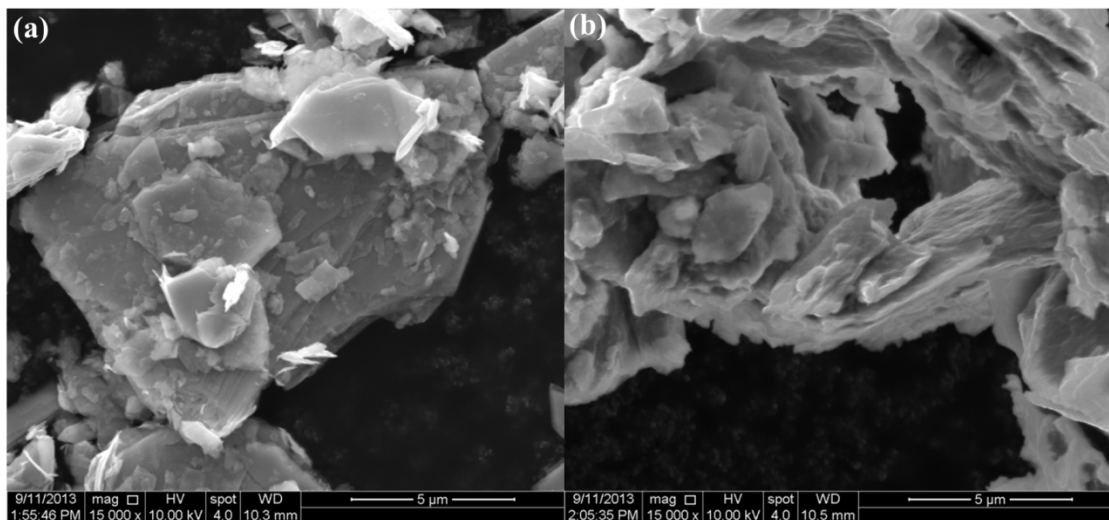

Figure 9. SEM images of (a) MoS_2 and (b) α phase intercalation compound $Na_{0.3}MoS_2 \cdot 0.4en$

Raman spectra of MoS_2 and a representative Na-en-MoS_2 intercalation compound are shown in Fig. 10. MoS_2 displays prominent sharp absorbance peaks at 390 cm^{-1} (E_{2g}^{1} mode) and 418 cm^{-1} (A_{2g} mode) as has been reported previously.[40, 41] After intercalation, the spectrum background increases significantly, the two sharp peaks broaden and shift slightly to lower frequency, and two new strong broad peaks appear at ≈1350 and ≈1600 cm^{-1}. Very similar changes were previously observed following Li intercalation into MoS_2, with the new high frequency peaks ascribed to a disordered state arising from intercalate arrangement.[41] In the present case, en has molecular absorbances in this region, however, these should be relatively sharp and the other strong en absorbances expected at 3300 ($\upsilon(NH_2)$), 2900 ($\upsilon(CH_2)$) and 2850 ($\upsilon(CH_2)$) cm^{-1} were not detected.[42] Therefore the high frequency broad bands present in the intercalation compound samples more likely arise from a transition associated with disorder within the intercalate galleries.
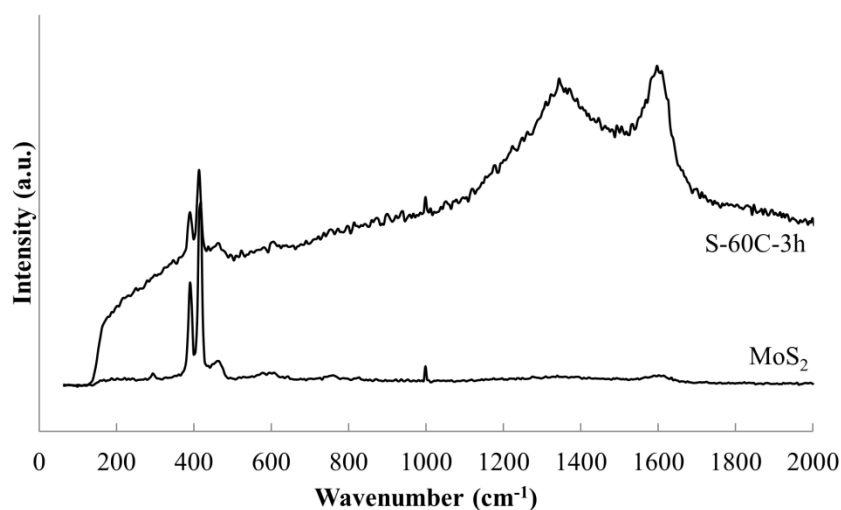

Figure 10. Raman spectra of MoS_2 and Na-en-MoS_2 intercalation
compound (S-60C-3h) indicates the structural change upon intercalation.

In contrast to the chemical syntheses, galvanostatic reduction of MoS_2 in en/$NaPF_6$ did not generate predominant intercalation products. A very weak XRD peak associated with the α phase is observed, but the principal change is a weakening and broadening of the MoS_2 host diffraction peaks (Figs. 11 and 12).
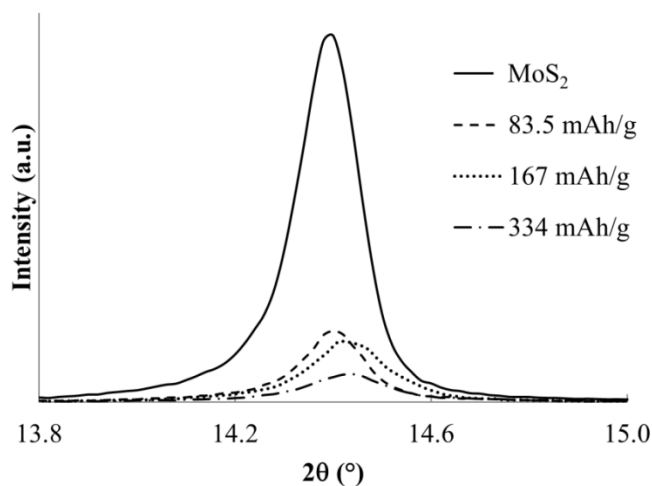
Figure 11. Powder XRD profiles for MoS_2 and products of electrochemical reduction in en/$NaPF_6$ with applied charges indicated.
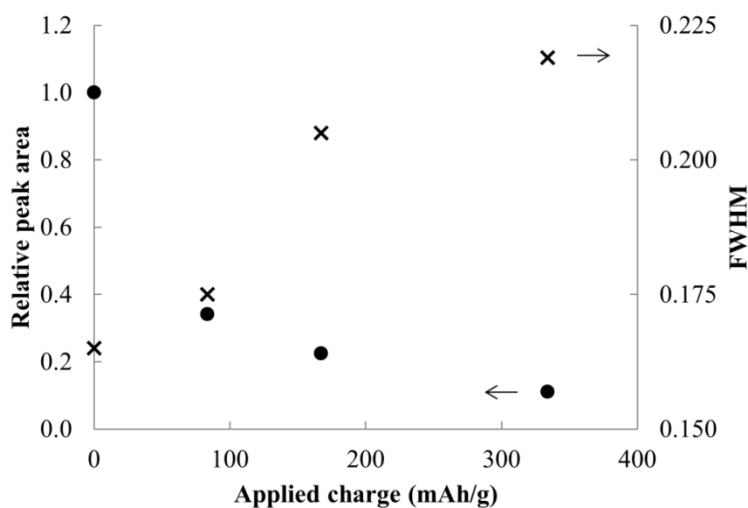

Figure 12. Relative peak areas and widths for MoS_2 and reduction products at different applied charges.

Lemmon et al reported that reduction of MoS_2 in a 7:3 vv ethylene methyl carbonate:ethylene carbonate electrolyte with $LiPF_6$ resulted in formation of Li_2S and an amorphous form of Mo or Li_xMo.[15, 16] The analogous reduction for Na reaction is in eqn (4):

$$MoS_2 + (4+x)Na^+ + (4+x)e^- \rightarrow 2\,Na_2S + Na_xMo \qquad (4)$$

Theoretically the capacity required for the above reduction is $\approx$840 mAh/g (if x=1); each 1e$^-$ reduction translates to 167 mAh/g. After applying from half to twice the latter charge, almost no intercalation products were evident. As can be seen, the ordered layered structure is destroyed even at much lower applied charges, suggesting an entirely different and non-intercalative mechanism for this electrochemical reduction.

Conclusions

MoS_2 reacts with electride solutions with amine to form intercalation compounds of composition $Na_{0.2-0.3}MoS_2\cdot 0.3-0.4en$. A metastable product, identified as the β phase, shows a perpendicular en orientation with interlayer expansion of 0.57 nm, and the thermodynamic product, or α phase, shows a parallel orientation and interlayer expansion of 0.35 nm. Shorter reaction time, dilution and lower temperatures favor formation of the β phase. The intercalation products are not obtained by electrochemical reduction in en/$NaPF_6$.

Acknowledgements

Corresponding Author

* Department of Chemistry, Oregon State University, Corvallis, OR, 97331-4003, United States. E-mail: michael.lerner@oregonstate.edu; Fax: (+1)-541-737-2062; Tel: (+1)-541-737-6747.

References

1. M. S. Whittingham and A. J. Jacobson, eds., *Intercalation Chemistry*, Academic Press, New York, NY., 1982.
2. F. A. Lévy, ed., *Intercalated layered materials*, D. Reidel Publishing, Dordrecht, Holland., 1979.
3. E. Benavente, M. A. Santa Ana, F. Mendizabal and G. Gonzalez, *Coordination Chemistry Reviews*, 2002, **224**, 87.
4. W. Rüdorff and H. H. Sick, *Angewandte Chemie*, 1959, **71**, 127.
5. W. Rüdorff, *Chimia*, 1965, **19**, 489.

6.   M. S. Whittingham and F. R. Gamble, *Materials Research Bulletin*, 1975, **10**, 363.

7.   R. B. Somoano, V. Hadek, A. Rembaum, S. Samson and J. A. Woollam, *Journal of Chemical Physics*, 1975, **62**, 1068.

8.   R. B. Somoano, V. Hadek and A. Rembaum, *Journal of Chemical Physics*, 1973, **58**, 697.

9.   M. A. Santa Ana, V. Sanchez and G. Gonzalez, *Electrochimica Acta*, 1995, **40**, 1773.

10.   A. A. Stepanov, N. D. Lenenko, A. S. Golub and V. S. Pervov, *Russian Journal of Electrochemistry*, 2013, **49**, 86.

11.   M. S. Whittingham, *Journal of Electroanalytical Chemistry*, 1981, **118**, 229.

12.   G. Gonzalez, M. A. Santa Ana and E. Benavente, *Electrochimica Acta*, 1998, **43**, 1327.

13.   V. Sanchez, E. Benavente, M. A. Santa Ana and G. Gonzalez, *Chemistry of Materials*, 1999, **11**, 2296.

14.   M. A. Lukowski, A. S. Daniel, F. Meng, A. Forticaux, L. S. Li and S. Jin, *Journal of the American Chemical Society*, 2013, **135**, 10274.

15.   J. Xiao, D. W. Choi, L. Cosimbescu, P. Koech, J. Liu and J. P. Lemmon, *Chemistry of Materials*, 2010, **22**, 4522.

16.   J. Xiao, X. J. Wang, X. Q. Yang, S. D. Xun, G. Liu, P. K. Koech, J. Liu and J. P. Lemmon, *Advanced Functional Materials*, 2011, **21**, 2840.

17.   L. David, R. Bhandavat and G. Singh, *ACS Nano*, 2014, **8**, 1759.

18.   G. S. Bang, K. W. Nam, J. Y. Kim, J. Shin, J. W. Choi and S.-Y. Choi, *ACS Applied Materials & Interfaces*, 2014, **6**, 7084.

19.   J. Park, J.-S. Kim, J.-W. Park, T.-H. Nam, K.-W. Kim, J.-H. Ahn, G. Wang and H.-J. Ahn, *Electrochimica Acta*, 2013, **92**, 427.

20.   J. L. Dye, *Science*, 2003, **301**, 607.

21.   E. Wein, W. Mullerwarmuth and R. Schöllhorn, *Solid State Ionics*, 1987, **22**, 231.

22.   L. Bernard, M. McKelvy, W. Glaunsinger and P. Colombet, *Solid State Ionics*, 1985, **15**, 301.

23.   L. A. Brown, W. S. Glaunsinger and M. J. McKelvy, *Journal of Solid State Chemistry*, 2000, **155**, 326.

24.   H. Ogata, H. Fujimori, S. Miyajima, K. Kobashi, T. Chiba, R. E. Taylor and K. Endo, *Journal of Physics and Chemistry of Solids*, 1997, **58**, 701.

25.   E. Figueroa, J. W. Brill and J. P. Selegue, *Journal of Physics and Chemistry of Solids*, 1996, **57**, 1123.

26.   H. Boller and H. Blaha, *Journal of Solid State Chemistry*, 1982, **45**, 119.

27.   M. S. Whittingham, *Materials Research Bulletin*, 1974, **9**, 1681.

28.   R. Schöllhorn and A. Weiss, *Journal of the Less-Common Metals*, 1974, **36**, 229.

29.   R. D. Shannon, *Acta Crystallographica Section A*, 1976, **32**, 751.

30.   O. Matsumoto, E. Yamada, Y. Kanzaki and M. Konuma, *Journal of Physics and Chemistry of Solids*, 1978, **39**, 191.

31.   T. Maluangnont, K. Gotoh, K. Fujiwara and M. M. Lerner, *Carbon*, 2011, **49**, 1040.

32.   T. Maluangnont, G. T. Bui, B. A. Huntington and M. M. Lerner, *Chemistry of Materials*, 2011, **23**, 1091.

33.   T. Maluangnont, M. M. Lerner and K. Gotoh, *Inorganic Chemistry*, 2011, **50**, 11676.
34.   T. Maluangnont, W. Sirisaksoontorn and M. M. Lerner, *Carbon*, 2012, **50**, 597.
35.   Y. H. Zhao, M. H. Abraham and A. M. Zissimos, *Journal of Organic Chemistry*, 2003, **68**, 7368.
36.   A. U. Liyanage and M. M. Lerner, *Rsc Advances*, 2012, **2**, 474.
37.   A. U. Liyanage, E. U. Ikhuoria, A. A. Adenuga, V. T. Remcho and M. M. Lerner, *Inorganic Chemistry*, 2013, **52**, 4603.
38.   J. Zheng, H. Zhang, S. H. Dong, Y. P. Liu, C. T. Nai, H. S. Shin, H. Y. Jeong, B. Liu and K. P. Loh, *Nature Communications*, 2014, **5**, 2995.
39.   A. Lerf and R. Schöllhorn, *Inorganic Chemistry*, 1977, **16**, 2950.
40.   C. N. R. Rao and A. Nag, *European Journal of Inorganic Chemistry*, 2010, 4244.
41.   T. Sekine, C. Julien, I. Samaras, M. Jouanne and M. Balkanski, *Materials Science and Engineering B-Solid State Materials for Advanced Technology*, 1989, **3**, 153.
42.   M. G. Giorgini, M. R. Pelletti, G. Paliani and R. S. Cataliotti, *Journal of Raman Spectroscopy*, 1983, **14**, 16.